Mechanism of sinuous and varicose modes in electrokinetic instability

Prateek Gupta
Department of Applied Mechanics, Indian Institute of Technology Delhi, New Delhi 110016, India

Supreet Singh Bahga*
Department of Mechanical Engineering, Indian Institute of Technology Delhi, Hauz Khas, New Delhi 110016, India

(Received 8 June 2024; accepted 30 August 2024; published 27 September 2024)

The flow of miscible electrolyte streams with mismatched electrical conductivities in the presence of a parallel applied electric field is known to exhibit electrokinetic instability (EKI). This paper deals with EKI in a configuration where the base state is established by electro-osmotic flow (EOF) of three coflowing streams, with the center stream having different conductivity than the sheath streams. All reported experiments of this EKI have shown that the instability exhibits either sinuous or varicose modes depending upon whether the center stream has higher or lower conductivity than the sheath streams, respectively. In this paper we elucidate the physical mechanism underlying the selection of these unstable modes in EKI using linear stability analysis. The stability analysis shows that the EOF simply convects the unstable modes besides establishing the base state. The instability occurs due to stationary convection cells, in the reference frame moving with the EOF, resulting from the coupling of the applied electric field with free charge in the regions with conductivity gradients. Importantly, we show that the unstable and stable disturbances for the configuration with a higher conductivity center stream have opposite stability characteristics when the center stream has lower conductivity than the sheath streams. Our analysis correctly explains the numerous experimental observations showing the consistent appearance of sinuous modes for higher conductivity and varicose modes for lower conductivity center streams.

DOI: 10.1103/PhysRevE.110.035106

I. INTRODUCTION

Electric field-driven fluid flow and ion transport have found widespread applications in microfluidic laboratory-on-a-chip systems [1,2]. The application of an external electric field through a microchannel can induce electro-osmotic flow (EOF), which is routinely used in pumping and precise control of fluids in microfluidic networks [2,3]. Moreover, ion transport driven by applied electric field forms the basis of numerous electrophoretic techniques for separating and preconcentrating ionic species [4,5]. Typically, in microfluidic systems such as micromixers and microchip electrophoresis, an electric field is applied through an electrolyte solution with heterogeneous electrical conductivity [6–8]. A gradient in electrical conductivity is accompanied by a gradient in the local electric field, which leads to the accumulation of free charge within the bulk liquid. This free charge couples with the local electric field to apply an electric body force on the fluid, which can destabilize the flow. Consequently, the application of an electric field above a critical value leads to an onset of electrohydrodynamic (EHD) instability of the bulk fluid [7,9–11].

EHD instability differs from EOF as the former is driven by the coupling of charges and electric field in the bulk solution, whereas EOF results from the Coulombic force on the free charges in the electrical double layer near a charged surface. We note that EHD instabilities can also occur in systems with immiscible fluid layers with unequal electrical properties [12,13]. In such systems, the electrohydrodynamic coupling occurs at the sharp interface separating the immiscible fluids. The current work deals with instability arising due to electrohydrodynamic coupling in bulk fluid due to diffusive conductivity gradients.

In many microfluidic systems, EHD instability is superimposed over EOF. The current work focuses on one such flow instability, which is employed in micromixers for rapid and chaotic mixing at low Reynolds numbers [14]. In particular, we consider a cross-shaped micromixer, described by Shin *et al.* [15] and Posner and Santiago [16], wherein EOF establishes a base-state flow with two sheath streams flowing in parallel with a center stream with mismatched conductivity. This results in a configuration where the applied electric field is orthogonal to the conductivity gradient, as illustrated in Fig. 1. Beyond a critical electric field, an EHD instability sets in, manifesting as either sinuous or varicose disturbances of the center stream, as illustrated in Figs. 1(b) and 1(c), respectively. In this case, the destabilizing flow is primarily due to the coupling of the electric field with bulk electrical conductivity gradients, and the EOF simply convects the unstable modes downstream [10,17]. However, given that EOF also establishes the base-state conductivity gradient and convects the unstable modes, such an EHD instability superimposed on EOF is often termed electrokinetic instability (EKI) [10,18]. While originally EKI in the flow configuration shown in Fig. 1 was motivated by rapid, chaotic micromixing [14], recently

*Contact author: bahga@mech.iitd.ac.in

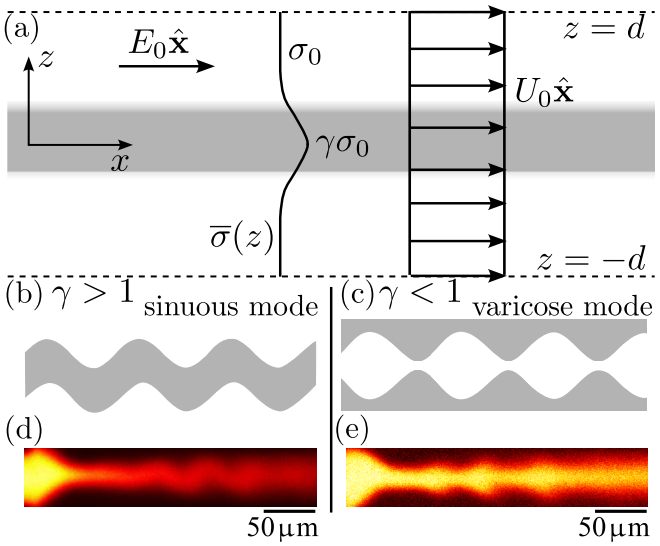

FIG. 1. Schematic illustrating the base state of EKI with coflowing sheath and center streams with different electrical conductivities. (a) The instability is driven by an electric field applied parallel to the diffused interfaces separating the streams with unequal conductivities. (b) When the center stream has higher conductivity than the sheath streams ($\gamma > 1$), EKI is characterized by a sinuous disturbance of the center stream. This corresponds to in-phase disturbances of the two diffusive interfaces. (c) In contrast, when a low-conductivity stream flows between high-conductivity sheath streams ($\gamma < 1$), the instability exhibits varicose disturbances of the center stream, corresponding to out-of-phase disturbances of the two diffusive interfaces. Panels (d) and (e) show the experimental snapshots of EKI, reproduced from Dubey *et al.* [19] showing sinuous and varicose modes for $\gamma > 1$ and $\gamma < 1$, respectively.

Dubey *et al.* [7] demonstrated experimentally that similar instability can arise in microchip electrophoresis with streamwise conductivity gradients, leading to undesirable sample dispersion.

EK instabilities driven by an electric field applied along a microchannel with spanwise conductivity gradients were first reported by Santiago and coworkers [6,10,16]. Using time-resolved imaging of a passive fluorescent scalar and linear stability analysis, they showed that the critical electric field above which EKI sets in is governed by the balance of destabilizing electro-viscous fluid motion and dissipation of conductivity gradients due to molecular diffusion. In particular, Posner and Santiago [16] presented a detailed experimental study of EKI in the flow configuration illustrated in Fig. 1, wherein the electric field is applied parallel to a high- (low-) conductivity stream flowing between two sheath streams with low (high) conductivity. Posner and Santiago showed that the characteristics of EKI depend on the relative conductivities of center and sheath streams. When the center stream has higher conductivity than the sheath streams, EKI is characterized by a sinuous (or wavy) mode, as shown in Figs. 1(b) and 1(d). On the other hand, if the center stream has lower conductivity than the sheath streams, a varicose (pearl-necklace) mode appears during the instability, as shown in Figs. 1(c) and 1(e). Later Dubey *et al.* [19] identified the spatiotemporal coherent structures corresponding to the sinuous and varicose modes of EKI using dynamic mode decomposition (DMD) of time-resolved snapshots. The experiments of Posner and Santiago [16] and Dubey *et al.* [19] also showed that the flow configuration with center stream having lower conductivity than the sheath streams requires a higher threshold electric field to destabilize, in comparison when high-conductivity stream flows between two low-conductivity sheath streams.

Despite the numerous experimental reports on sinuous and varicose modes of EKI for different base-state flows, the physical mechanism underlying the selection of these distinct instability modes is still poorly understood. Specifically, there has been no linear stability analysis of EKI in the configuration with two parallel diffusive interfaces to elucidate the mode selection mechanism based on the relative conductivities of the flow streams. All the reported linear stability analyses of EHD and EK instabilities, including those by Hoburg and Melcher [9], Chen *et al.* [10], and Patankar [17], are limited to a single diffusive interface between streams with unequal conductivities stressed under a tangential electric field. The stability analyses presented in these works suggest that a small sinusoidal perturbation of a single diffusive interface drives a cellular flow that further amplifies the conductivity perturbation. A naive application of this mechanism for the flow configuration with two parallel diffusive interfaces, as shown in Fig. 1, would suggest that the instability can set in with in-phase and out-of-phase perturbations of the two parallel interfaces, corresponding to sinuous and varicose modes, respectively. However, extensive experimental data in the literature suggests a selection of unstable modes in EKI [16,19], depending upon the relative conductivities of the center and sheath streams.

In this paper, we describe the physical mechanism underlying the selection of sinuous and varicose modes in EKI instability, using linear stability analysis, in a flow configuration with two sheath streams coflowing with a center stream with different conductivity. The stability analysis correctly predicts experimentally observed sinuous (varicose) modes of EKI when the center stream has high (low) conductivity compared with the sheath streams. Moreover, we show that EKI exhibits these modes irrespective of the difference in the conductivities of center and sheath streams. Finally, using a simplified model of EKI in the limit of small conductivity difference between the flow streams, we describe the instability dynamics and the physics underlying the selection of unstable modes.

II. DESCRIPTION OF FLOW

Figure 1 illustrates the flow configuration of EKI that we model in the current work. An externally applied electric field $E_0\hat{\mathbf{x}}$ drives a uniform EOF with velocity $U_0\hat{\mathbf{x}}$. The EOF establishes a base-state flow with coflowing center and sheath streams with different electrical conductivities. The coupling of the electric field with bulk electrical conductivity gradients destabilizes the flow and results in EKI. Before presenting the mathematical modeling of the EKI in the flow configuration depicted in Fig. 1, it is meaningful to discuss the typical values of various physical quantities in microfluidic EKI experiments [16,19] and the simplifications we make to elucidate the basic physics of the instability.

Typically, EKI experiments are performed in a glass microchannel with a width and depth of O(10–100 μm) . For our discussion, we consider the channel half-width to be $d = 25$ μm. The axial length of the microchannel is O(1 cm) or more, that is, at least two orders of magnitude larger than the channel width. The conductivity gradient is generated by coflowing aqueous electrolyte solutions with different salt concentrations. The typical salt concentration is O(1–10 mM), which corresponds to an electrical conductivity of O(0.05–0.5 S m^{-1}). The density, viscosity, and electrical permittivity of such dilute electrolytes can be assumed to be those of pure water.

In the base state, the spatial conductivity variation is governed by the balance of convection due to EOF and diffusion. The typical diffusivity of the salt ions and, correspondingly, the effective diffusivity D of the conductivity is $O(10^{-9}$ m^2 s$^{-1})$. In EKI experiments, an axial electric field $E_0\hat{\mathbf{x}}$ of O(10 kV m^{-1}) is applied by applying a voltage difference of O(100 V) across O(1 cm) long microchannel. This electric field couples with the thin electric double layer [thickness O(10 nm)] near the microchannel walls to drive an EOF [20]. Because the electric double layer is three orders of magnitude smaller than the channel width, the EOF appears to slip at the channel walls. The EOF slip velocity due to an axially uniform tangential electric field at the walls results in a plug-shaped velocity profile, given by $U_0\hat{\mathbf{x}}$, as shown in Fig. 1, where $U_0 = \mu_{\rm eof}E_0$. Here $\mu_{\rm eof}$ is the EOF mobility and for a glass microchannel, its typical value is $\mu_{\rm eof} = 7 \times 10^{-8}$ m^2 V^{-1} s^{-1} [20,21]; that is, the applied electric field of O(10 kV m^{-1}) results in an EOF velocity of O(0.7 mm s^{-1}). Therefore, the Péclet number $\mathrm{Pe} = U_0 d/D$ for convection diffusion of conductivity field is at least O(10). In other words, the axial convection of conductivity due to EOF dominates spanwise diffusion. Hence, the conductivity variation along the axial (x) direction is significantly small, and the base-state conductivity variation can be assumed to be uniform in the x direction. Consequently, the axial length of the microchannel drops out of the analysis.

We also assume that the flow is two-dimensional so as to focus on describing the physical mechanism of EKI. The presence of walls along the depth direction increases the viscous stresses, due to which a higher threshold electric field is required to destabilize the flow [22]. However, numerical simulations and stability analysis of EKI in various configurations [7,22] suggest the basic physical mechanism of EKI is the same for two- and three-dimensional configurations. Finally, we note that measurements and modeling of Joule heating in electrokinetic flow experiments with aforementioned values of physical parameters have shown that the temperature rise of the fluid is about 2 °C [10,23]. Therefore, it is reasonable to assume a constant temperature in the mathematical model.

III. MATHEMATICAL MODELLING

With the above assumptions, we consider the instability of two-dimensional, planar, coflowing center and sheath streams between boundaries at $z = \pm d$ that extend infinitely in the y direction, as shown in Fig. 1. An external electric field $E_0\hat{\mathbf{x}}$ is applied along the x direction. The axial electric field drives an EOF with uniform velocity $U_0\hat{\mathbf{x}}$, which convects the center and sheath streams. The diffusive interfaces separating the center and sheath streams are idealized to be parallel to the x direction. That is, the electric field is parallel to the two diffusive interfaces separating the flow streams. We assume the center and sheath fluids to be binary electrolyte solutions of the same salt but with different concentrations.

A. Governing equations

The incompressible flow of a fluid driven by the coupling of an applied electric field and diffusive conductivity gradients is governed by the following continuity and momentum equations [10,11]:

$$\nabla \cdot \mathbf{u} = 0, \tag{1}$$

$$\rho\frac{\partial \mathbf{u}}{\partial t} + \rho\mathbf{u}\cdot\nabla\mathbf{u} = -\nabla p + \eta\nabla^2\mathbf{u} + \epsilon(\nabla\cdot\mathbf{E})\mathbf{E}. \tag{2}$$

Here $\mathbf{u}$ denotes the flow velocity, $\mathbf{E}$ the local electric field, p the pressure, and ρ and η denote the density and dynamic viscosity of the liquid, respectively. Equation (2) is the Navier-Stokes momentum equation with an additional electric body force term $\rho_f\mathbf{E}$, where ρ_f denotes the free charge in the bulk liquid. For a linear dielectric liquid with spatially uniform dielectric permittivity ϵ, the free charge is given by Gauss' law $\rho_f = \epsilon\nabla\cdot\mathbf{E}$. Hence, the electric body force in the momentum equation, Eq. (2), is given by $\rho_f\mathbf{E} = \epsilon(\nabla\cdot\mathbf{E})\mathbf{E}$.

The local electric field $\mathbf{E}$ is governed by the continuity of current or Ohm's law,

$$\nabla\cdot(\sigma\mathbf{E}) = 0, \tag{3}$$

where σ denotes the local electrical conductivity of the liquid. This equation holds for electrolyte solutions, assuming the bulk solution is approximately electroneutral [10,11]. In addition, we note that for low current density and displacement current $\partial(\epsilon\mathbf{E})/\partial t$, the electric field can be assumed to be quasistatic. Hence, from Maxwell's equations

$$\nabla\times\mathbf{E} = \mathbf{0}. \tag{4}$$

Because the electric field is irrotational, we can express the electric field in terms of an electric potential ϕ, as $\mathbf{E} = -\nabla\phi$.

Finally, the transport of electrical conductivity can be derived from the mass conservation equations of cations and anions of a symmetric-binary electrolyte, assuming the bulk solution to be electroneutral [11,24]. The resulting convection-diffusion equation for the electrical conductivity is given by

$$\frac{\partial\sigma}{\partial t} + \mathbf{u}\cdot\nabla\sigma = D\nabla^2\sigma, \tag{5}$$

where D is the diffusivity.

Equations (1)–(5) describe the EHD flow of a symmetric binary electrolyte having diffusive conductivity gradients. We note that these equations are based on the assumption that the difference between the electrolyte's cation and anion concentrations is negligible compared to their bulk concentrations. This assumption is valid when the charge-relaxation timescale $\tau_r = \epsilon/\sigma$ is significantly smaller than other timescales in the flow [9]. For EKI, the charge relaxation timescale $\tau_r \sim O$(10 ns), and hence the assumption of a nearly electroneutral solution is valid. Despite an almost electroneutral solution, the

free charge associated with a small difference between cation and anion concentrations is sufficient to exert an appreciable body force in the fluid [10], which is incorporated in the momentum equation, Eq. (2).

Because we assume an approximately electroneutral solution, the free charge density is not obtained using the ion concentrations. Instead, we use Ohm's law, given by Eq. (3), to obtain the electric field $\mathbf{E}$ and thereafter, the free charge density ρ_f is obtained using Gauss' law. Therefore, using Ohm's law (Eq. (3)) and Gauss' law $\rho_f = \epsilon \boldsymbol{\nabla} \cdot \mathbf{E}$, the free charge density can be expressed as

$$\rho_f = -\epsilon \mathbf{E} \cdot \boldsymbol{\nabla}\sigma/\sigma. \tag{6}$$

This equation suggests that the polarity of charge accumulated in the bulk solution is opposite to the sign of the directional derivative of σ along $\mathbf{E}$.

B. Base state

For stability analysis, we consider the evolution of small disturbances over the base state illustrated in Fig. 1. For the typical experimental conditions described in Sec. II, the steady, base-state conductivity distribution, $\overline{\sigma}$, establishes due to the dominant balance of streamwise convection due to EOF and spanwise diffusion. That is, the conductivity transport equation, Eq. (5), for base-state conductivity $\overline{\sigma}$ can be simplified as

$$U_0 \frac{\partial \overline{\sigma}}{\partial x} \approx D \frac{\partial^2 \overline{\sigma}}{\partial z^2}. \tag{7}$$

We assume that the base-state conductivity distribution develops from a narrow top-hat distribution centered at $z = 0$, starting from $x = 0$, upstream of the region of interest. For the case where the spanwise diffusion length is much larger than the initial width of the top-hat conductivity distribution but smaller than the channel width, Eq. (7) has a solution of the form

$$\frac{\overline{\sigma}(z)}{\sigma_0} = 1 + \frac{A}{\delta} \exp\left(-\frac{z^2}{2\delta^2}\right), \quad \delta = \sqrt{\frac{2Dx}{U_0}}. \tag{8}$$

Here σ_0 is the conductivity of the sheath streams, and A is a constant dependent on the inlet conductivity distribution. In the high Péclet number limit, $U_0 d/D \gg 1$, which is the case for EKI experiments, the conductivity variation given by Eq. (8) varies slowly with x for $x \gg d$. Therefore, we can idealize the base-state electrical conductivity to vary in the transverse (z) direction only with a constant δ,

$$\frac{\overline{\sigma}(z)}{\sigma_0} = 1 + (\gamma - 1) \exp\left(-\frac{z^2}{2\delta^2}\right). \tag{9}$$

Here γ is the ratio of conductivities of the center and sheath streams, and σ_0 is the conductivity of the sheath streams. For all our calculations, we consider $\delta = d/4$, for which the conductivity gradients near the domain boundaries $z = \pm d$ are negligible. Also, being far from the inlet of the channel, we assume the domain of analysis to extend infinitely in both positive and negative directions along the x axis.

C. Dimensionless governing equations

Prior to linear stability analysis, we nondimensionalize the governing equations, Eqs. (1)–(5), using the following reference scales:

$$[x, y, z] = d, \quad [\mathbf{E}] = E_0, \quad [\phi] = E_0 d, \quad [\mathbf{u}] = U_{ev},$$
$$[t] = \frac{d}{U_{ev}}, \quad [p] = \epsilon E_0^2, \quad [\rho_f] = \frac{\epsilon E_0}{d}, \quad [\sigma] = \sigma_0. \tag{10}$$

Here $U_{ev} = \epsilon E_0^2 d/\eta$ is the electroviscous velocity scale obtained by balancing the electric body force and viscous stresses [9,10]. Upon nondimensionalizing the governing equations, Eqs. (1)–(5), using these reference scales and using $\mathbf{E} = -\boldsymbol{\nabla}\phi$ we obtain the following set of dimensionless governing equations:

$$\boldsymbol{\nabla} \cdot \mathbf{u} = 0, \tag{11}$$

$$\frac{\mathrm{Ra}_e}{\mathrm{Sc}}\left[\frac{\partial \mathbf{u}}{\partial t} + \mathbf{u} \cdot \boldsymbol{\nabla}\mathbf{u}\right] = -\boldsymbol{\nabla} p + \nabla^2 \mathbf{u} + (\nabla^2 \phi)\boldsymbol{\nabla}\phi, \tag{12}$$

$$\boldsymbol{\nabla} \cdot (\sigma \boldsymbol{\nabla}\phi) = 0, \tag{13}$$

$$\frac{\partial \sigma}{\partial t} + \mathbf{u} \cdot \boldsymbol{\nabla}\sigma = \frac{1}{\mathrm{Ra}_e} \nabla^2 \sigma. \tag{14}$$

Here $\mathrm{Ra}_e = \epsilon E_0^2 d^2/(\eta D)$ is the electric Rayleigh number and $\mathrm{Sc} = \eta/(\rho D)$ is the Schmidt number. In Eqs. (11)–(14), $\mathbf{u}$, p, ϕ, and σ denote the dimensionless velocity, pressure, electric potential, and conductivity, respectively. Henceforth, we use only the dimensionless variables in our analysis.

The electric Rayleigh number appearing in the governing equations is the ratio of timescales associated with the diffusion of conductivity ($\tau_d = d^2/D$) and the convection due to electroviscous flow [$\tau_{ev} = d/U_{ev} = \eta/(\epsilon E_0^2)$]; that is, $\mathrm{Ra}_e = \tau_d/\tau_{ev}$. In EKI, diffusion stabilizes the flow because it dissipates the conductivity gradients responsible for charge accumulation in the bulk fluid. Therefore, instability occurs when the destabilizing electroviscous flow stretches the conductivity gradients faster than diffusion dissipates them, that is, $\tau_{ev} \ll \tau_d$. In other words, linear stability analysis should predict a threshold value of $\mathrm{Ra}_e \gg 1$ above which the instability occurs, as observed in experiments [16,19].

D. Linear stability analysis

In the base state, illustrated in Fig. 1, the dimensionless velocity, electric potential, and pressure are given by

$$\overline{\mathbf{u}} = U\hat{\mathbf{x}}, \quad \overline{\phi} = -x, \quad \overline{p} = 0, \tag{15}$$

where $U = U_0/U_{ev}$. The base-state conductivity $\overline{\sigma}$ upon nondimensionalizing Eq. (9), is given by

$$\overline{\sigma}(z) = 1 + (\gamma - 1)\exp(-8z^2). \tag{16}$$

Note that there is no free charge in the base state because, in the base state, the applied electric field is parallel to the diffusive interfaces separating the streams with mismatched conductivities.

To perform linear stability analysis, we model the behavior of small two-dimensional disturbances over the base state.

Therefore, we decompose the variables in terms of their base state and perturbation (denoted by primes) values,

$$\mathbf{u} = \overline{\mathbf{u}} + \mathbf{u}', \quad \phi = \overline{\phi} + \phi', \quad p = \overline{p} + p', \quad \sigma = \overline{\sigma} + \sigma'. \tag{17}$$

Upon substituting these variables in the dimensionless governing equations, Eqs. (11)–(14), and neglecting the higher-order terms in perturbation variables, we obtain a set of linearized governing equations for perturbation variables,

$$\nabla \cdot \mathbf{u}' = 0, \tag{18}$$

$$\frac{\mathrm{Ra}_e}{\mathrm{Sc}}\left[\frac{\partial \mathbf{u}'}{\partial t} + U\frac{\partial \mathbf{u}'}{\partial x}\right] = -\nabla p' + \nabla^2 \mathbf{u}' - (\nabla^2 \phi')\hat{\mathbf{x}}, \tag{19}$$

$$\nabla \cdot (\overline{\sigma}\nabla\phi') - \frac{\partial \sigma'}{\partial x} = 0, \tag{20}$$

$$\frac{\partial \sigma'}{\partial t} + U\frac{\partial \sigma'}{\partial x} + w'\frac{d\overline{\sigma}}{dz} = \frac{1}{\mathrm{Ra}_e}\nabla^2\sigma'. \tag{21}$$

Here w' denotes the z component of the perturbation velocity and $\nabla^2 \equiv \partial^2/\partial x^2 + \partial^2/\partial z^2$.

To simplify the governing equations for perturbation variables, we express the perturbation velocity $\mathbf{u}' = u'\hat{\mathbf{x}} + w'\hat{\mathbf{z}}$ in terms of a streamfunction $\psi'(x, z, t)$ as

$$u' = \frac{\partial \psi'}{\partial z}, \quad w' = -\frac{\partial \psi'}{\partial x}, \tag{22}$$

which by definition satisfies the continuity equation, Eq. (18). Next, to eliminate pressure from the momentum equation, we take the curl of Eq. (19) to get

$$\frac{\mathrm{Ra}_e}{\mathrm{Sc}}\left[\frac{\partial}{\partial t} + U\frac{\partial}{\partial x}\right]\nabla^2\psi' = \nabla^4\psi' - \frac{\partial}{\partial z}\nabla^2\phi'. \tag{23}$$

Equations (21) and (23) describe the evolution of conductivity and velocity perturbations, while Eq. (20) describes the variation of electric potential due to the conductivity disturbance. Equations (21) and (23) suggest that the role of base-state EOF velocity, $U\hat{\mathbf{x}}$, is to simply convect the velocity and conductivity disturbances. Therefore, to study the destabilizing EHD flow and its underlying physical mechanism, it is convenient to express the governing equations in a reference frame moving with the uniform base-state flow. Henceforth, denoting x to be the axial coordinate in the reference frame translating at the base-state velocity $U\hat{\mathbf{x}}$, the governing equations in the moving frame are given by

$$\frac{\mathrm{Ra}_e}{\mathrm{Sc}}\frac{\partial}{\partial t}(\nabla^2\psi') = \nabla^4\psi' - \frac{\partial}{\partial z}\nabla^2\phi', \tag{24}$$

$$\nabla \cdot (\overline{\sigma}\nabla\phi') - \frac{\partial \sigma'}{\partial x} = 0, \tag{25}$$

$$\frac{\partial \sigma'}{\partial t} - \frac{\partial \psi'}{\partial x}\frac{d\overline{\sigma}}{dz} = \frac{1}{\mathrm{Ra}_e}\nabla^2\sigma'. \tag{26}$$

To solve the governing equations, Eqs. (24)–(26), we require one boundary condition for ϕ' and σ', and two boundary conditions for ψ' at each boundary, $z = \pm 1$. Because the conductivity at the boundaries is maintained constant by the sheath streams, we assume that the conductivity perturbations vanish at $z = \pm 1$. Consequently, the perturbations in the electric field also vanish at the boundaries. These boundary conditions can be expressed as

$$\sigma' = 0 \text{ and } \frac{\partial \phi'}{\partial z} = 0 \quad \text{at} \quad z = \pm 1. \tag{27}$$

The remaining boundary conditions can be obtained by considering that the velocity perturbations vanish at the boundaries and assuming the boundaries to be stress-free [25],

$$\psi' = \frac{\partial^2 \psi'}{\partial z^2} = 0 \quad \text{at} \quad z = \pm 1. \tag{28}$$

E. Normal mode analysis

The governing equations, Eqs. (24)–(26), and the boundary conditions (27) and (28) are linear. Therefore, we can analyze the temporal evolution of individual perturbations using the normal mode analysis. To this end, we consider the perturbation variables of the form

$$\begin{Bmatrix} \psi'(x,z,t) \\ \phi'(x,z,t) \\ \sigma'(x,z,t) \end{Bmatrix} = \begin{Bmatrix} \hat{\psi}(z) \\ \hat{\phi}(z) \\ \hat{\sigma}(z) \end{Bmatrix} \exp(st + ikx), \tag{29}$$

where s and k denote the dimensionless growth rate and wave number, respectively. In general, the growth rate can be complex-valued, that is, $s = \mathrm{Re}(s) + i\mathrm{Im}(s)$. Substituting the form of solution given by Eq. (29) in the governing equations, Eqs. (24)–(26), yields a coupled set of ordinary differential equations in $\hat{\psi}$, $\hat{\phi}$, and $\hat{\sigma}$,

$$\frac{s\mathrm{Ra}_e}{\mathrm{Sc}}(D^2 - k^2)\hat{\psi} = (D^2 - k^2)^2\hat{\psi} - (D^2 - k^2)D\hat{\phi}, \tag{30}$$

$$\overline{\sigma}(D^2 - k^2)\hat{\phi} + D\overline{\sigma}D\hat{\phi} - ik\hat{\sigma} = 0, \tag{31}$$

$$s\hat{\sigma} - ikD\overline{\sigma}\hat{\psi} = \frac{1}{\mathrm{Ra}_e}(D^2 - k^2)\hat{\sigma}, \tag{32}$$

where $D \equiv d/dz$. Similarly, the boundary conditions (27) and (28) simplify to

$$\hat{\psi} = D^2\hat{\psi} = D\hat{\phi} = \hat{\sigma} = 0 \quad \text{at} \quad z = \pm 1. \tag{33}$$

Equations (30)–(32) along with the boundary conditions (33) define an eigenvalue problem with growth rates s as the eigenvalues and $\hat{\psi}$, $\hat{\phi}$, and $\hat{\sigma}$ as the corresponding eigenmodes. To solve this eigenvalue problem, we use the pseudospectral collocation method with Chebyshev polynomials as the basis functions [26]. We used 70 terms of the Chebyshev polynomials for all our calculations, beyond which there was negligible change in the computed eigenvalues.

IV. RESULTS AND DISCUSSION

In this section, we present the results of linear stability analysis for flow configurations with varying center-to-sheath stream conductivities. For all our calculations, we used $\mathrm{Sc} = 1000$, corresponding to a typical EKI experiment with aqueous electrolytes, having $\eta = 10^{-3}$ Pa s, $\rho = 1000$ kg m^{-3}, and $D = 10^{-9}$ m^2 s^{-1}. Using these values of physical properties and taking $\epsilon = 6.9 \times 10^{-10}$ C V^{-1} m^{-1}, $d = 25$ μm and microchannel length of 1 cm, an applied voltage difference of 500 V across the microchannel corresponds to $\mathrm{Ra}_e \approx 1000$.

First, we present the neutral stability curves and the eigenmodes corresponding to the critical states for the onset of

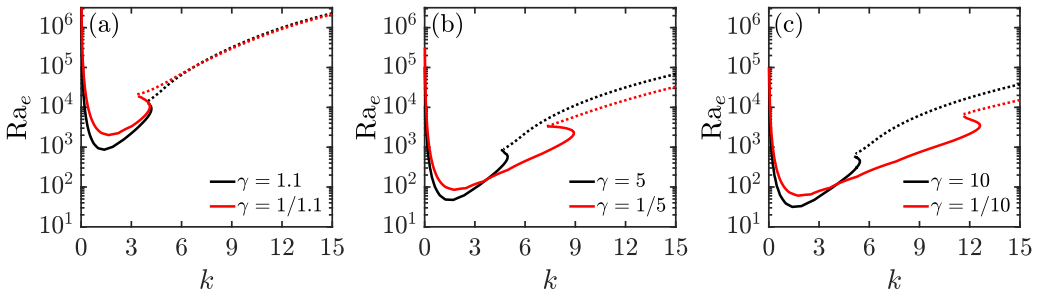

FIG. 2. Neutral stability curves for EKI in flow configuration wherein high- (low-) conductivity center stream coflows between low- (high-) conductivity sheath streams. The conductivity ratio $\gamma > 1$ corresponds to the higher conductivity of the center stream compared with the sheath streams, while $\gamma < 1$ corresponds to the opposite configuration. The solid lines denote the neutral states that exhibit a stationary eigenmode, while the dotted lines denote the neutral states corresponding to an oscillatory eigenmode. The critical states exhibit a stationary mode for all conductivity ratios and flow configurations.

instability. We also present a qualitative comparison of the critical modes with those observed in the reported experiments. We then present an approximate set of governing equations assuming a small conductivity difference between the center and sheath streams. Finally, using the approximate model, we present the physical mechanism of the selective appearance of the sinuous and varicose modes of EKI for different flow configurations.

A. Neutral stability

First, we present the neutral stability curves corresponding to Ra_e and k values for which the real part of the leading eigenvalue is zero, $\mathrm{Re}(s) = 0$. We computed the neutral stability curves for two types of base-state flows: (i) where high-conductivity center stream coflows with low-conductivity sheath streams ($\gamma > 1$) and (ii) where the center stream has lower conductivity than the sheath streams ($\gamma < 1$). In Fig. 2, we present the neutral stability curves for the two configurations for varying values of conductivity ratio γ. The solid lines in Fig. 2 correspond to the neutral states that exhibit a stationary eigenmode, that is, with $\mathrm{Im}(s) = 0$ besides $\mathrm{Re}(s) = 0$. On the other hand, the dotted lines denote the neutral states corresponding to an oscillatory eigenmode with $\mathrm{Im}(s) \neq 0$. The oscillatory eigenmodes occur in a pair with a complex conjugate pair of growth rates with identical $\mathrm{Re}(s)$.

The neutral stability curve for the center-to-sheath stream conductivity ratio of $\gamma = 1.1$ is shown in Fig. 2(a). The EKI sets in as a stationary mode at low wave numbers k, while at higher wave numbers, the neutral states exhibit an oscillatory mode. Importantly, the critical state ($k = 1.1$, $\mathrm{Ra}_e = 863.27$), corresponding to the minima of the neutral stability curve, exhibits a stationary eigenmode. Figure 2(a) also shows the neutral curve for the case wherein the center and sheath streams are interchanged, that is, when the center-to-sheath stream conductivity ratio is $\gamma = 1/1.1$. The neutral curve for $\gamma = 1/1.1$ is qualitatively similar to that for $\gamma = 1.1$. However, the critical state for $\gamma = 1/1.1$ occurs at a higher value of Ra_e. This prediction is consistent with the observations of Posner and Santiago [16] and Dubey *et al.* [19], whose experiments showed that EKI occurs at higher electric field for the flow configuration with low-conductivity stream flowing between two high-conductivity sheath streams, compared with the opposite configuration.

In Figs. 2(b) and 2(c), we present similar neutral curves for $\gamma = 5, 1/5, 10$, and $1/10$. These neutral curves are qualitatively similar to those presented in Fig. 2(a) for $\gamma = 1.1$ and $1/1.1$. However, consistent with the experimental observations [16], the critical Ra_e decreases with an increase in the mismatch between electrical conductivities of center and sheath streams. A larger difference between the center and sheath stream conductivities leads to a stronger electric body force, destabilizing the flow at a lower electric field and Ra_e.

The neutral stability curves for different conductivity ratios γ, shown in Fig. 2, suggest that the critical mode is stationary, irrespective of the conductivity ratio; that is, in the reference frame moving with EOF, the critical mode does not propagate in the axial direction (x direction). In other words, the convection of unstable modes in EKI is solely due to EOF, while the destabilizing mechanism is purely electrohydrodynamic in nature.

Another interesting observation from Fig. 2 is that the neutral stability curves for this instability with orthogonal conductivity gradients and electric field are qualitatively similar to those for EHD instability with a colinear conductivity gradient and electric field [11,27]. However, in the latter configuration, the critical mode is stationary only for a high-base-state conductivity gradient, and for a base state with a low-conductivity gradient, the critical mode is oscillatory. In contrast, in the present case, our calculations show that the critical mode is stationary for all conductivity ratios. Consequently, setting $s = 0$ in the governing equations, Eqs. (30)–(32), shows that the critical state and the corresponding modes are independent of the Schmidt number Sc.

B. Critical modes

Next, we present the eigenmodes corresponding to the critical states for representative center-to-sheath stream conductivity ratios of $\gamma = 1.1, 1/1.1, 10$, and $1/10$. In Fig. 3 we present the critical eigenmodes for conductivity σ' along with the corresponding streamlines ψ'. Figures 3(a) and 3(b), respectively, show the critical modes for $\gamma = 1.1$ and 10, that is, for cases where the center stream has higher conductivity than the sheath streams. The critical modes for $\gamma = 1.1$ and 10 are qualitatively similar but differ in their wave number k and the corresponding critical Ra_e. For $\gamma = 1.1$ the critical state occurs at $k = 1.33$ and $\mathrm{Ra}_e = 863.27$, while for

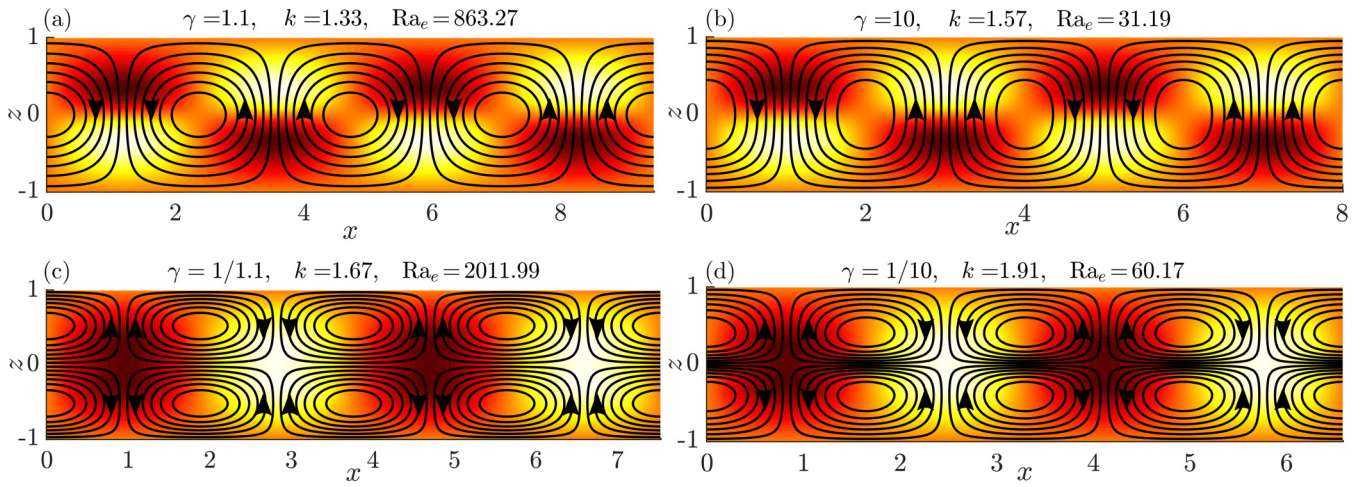

FIG. 3. The eigenmodes for conductivity σ' and the streamlines ψ' corresponding to the critical states for $\gamma = 1.1$, $1/1.1$, 10, and $1/10$. Yellow and red correspond to positive and negative perturbations, respectively. Panels (a) and (b) show sinuous conductivity disturbances for $\gamma = 1.1$ and 10, respectively. Panels (c) and (d) show varicose conductivity disturbances for $\gamma = 1/1.1$ and $1/10$, respectively. The convection cells indicate a destabilizing EHD flow, which further amplifies the conductivity disturbances.

$\gamma = 10$ the critical state occurs at $k = 1.57$ and $\mathrm{Ra}_e = 31.19$. Importantly, Figs. 3(a) and 3(b) show that for $\gamma > 1$, the instability is characterized by conductivity perturbations that are antisymmetric about the center line ($z = 0$). These antisymmetric conductivity perturbations correspond to sinuous (in-phase) disturbances of the diffusive interfaces separating center and sheath streams. The streamlines show that these sinuous conductivity disturbances are accompanied by stationary convection cells that span the thickness of the fluid layer and are symmetric about the center line ($z = 0$). These streamlines depict a flow field that further stretches the conductivity disturbances, suggesting the destabilizing nature of the EHD flow.

In Figs. 3(c) and 3(d) we present the critical eigenmodes of conductivity and the corresponding streamlines for $\gamma = 1/1.1$ and $1/10$, respectively, that is, for cases when the center stream has lower conductivity than the sheath streams. The critical state for $\gamma = 1/1.1$ occurs at $k = 1.67$ and $\mathrm{Ra}_e = 2011.99$, while that for $\gamma = 1/10$ occurs at $k = 1.91$ and $\mathrm{Ra}_e = 60.17$. For $\gamma < 1$, the critical eigenmodes of conductivity, shown in Figs. 3(c) and 3(d), exhibit symmetric disturbances about the center line. These symmetric conductivity disturbances correspond to the varicose (out-of-phase) disturbances of the diffusive interfaces separating the center and sheath streams. The streamlines corresponding to the critical state for $\gamma < 1$ show a pair of counter-rotating convection cells along the thickness of the fluid layer. The flow field associated with these convection cells tends to further amplify the conductivity disturbances.

The critical modes of conductivity shown in Fig. 3 bear a striking resemblance with the DMD modes extracted from experimental data of EKI by Dubey *et al.* [19]. Further, for a qualitative visual comparison of sinuous and varicose modes with experimental observations, in Fig. 4 we replot the critical modes of conductivity perturbation σ' for $\gamma = 1.1$ and $\gamma = 1/1.1$ (shown in Fig. 3) by superimposing them on the corresponding base-state conductivity field. In this figure, we have adjusted the contour colors to ensure the center stream appears dyed with a passive fluorescent scalar, as in the experiments [16,19]. The conductivity fields shown in Figs. 4(a) and 4(b) compare well with the experimental snapshots shown in Figs. 1(d) and 1(e), respectively. Overall, the linear stability analysis correctly predicts the experimentally observed sinuous and varicose modes of EKI for different base-state flows.

C. Limit of small conductivity difference between the center and sheath streams

We have shown that the linear stability analysis correctly predicts the sinuous and varicose EKI modes observed in the experiments. However, the analysis till now does not explain

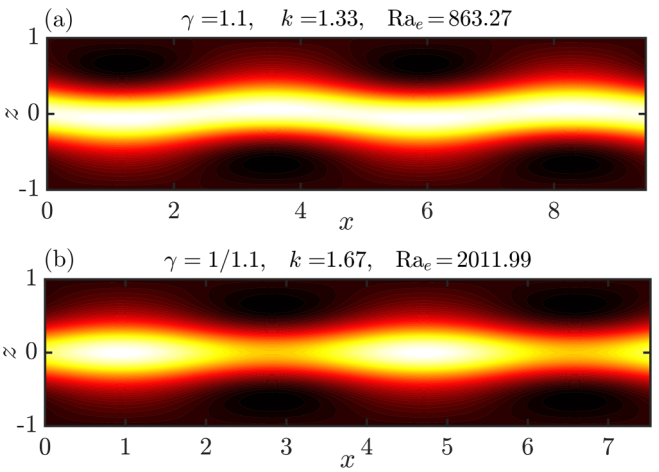

FIG. 4. Conductivity fields predicted using linear stability analysis at critical states for $\gamma = 1.1$ and $\gamma = 1/1.1$. These plots were generated by superimposing the critical modes of perturbation conductivity σ' on the corresponding base-state conductivity fields. The contour colors have been adjusted to ensure the center stream appears dyed with a passive fluorescent scalar, as in the experiments. (a) Sinuous disturbance of the center stream for $\gamma = 1.1$; (b) varicose disturbance of the center stream for $\gamma = 1/1.1$.

why EKI in a given configuration exhibits a particular mode (sinuous or varicose) and not the other mode. To elucidate the physical mechanism underlying the selection of unstable modes, we simplify the governing equations, Eqs. (24)–(26), in the limit of vanishingly small conductivity difference between the center and sheath streams, that is, $\gamma = 1 + \alpha$, where $|\alpha| \ll 1$. This assumption is particularly justified to explain the physical mechanism because the neutral stability curves and the critical modes presented in Secs. IV A and IV B show that the stability characteristics and the critical modes are qualitatively similar for varying conductivity differences between the center and sheath streams.

In the limit of small conductivity difference between the flow streams, we can perform regular asymptotic analysis of the linearized governing equations, Eqs. (24)–(26), taking $\alpha = \gamma - 1$ as the small parameter. We expand ψ', ϕ', and σ' as follows:

$$\psi' = \psi'_0 + \alpha\psi'_1 + O(\alpha^2), \quad \phi' = \phi'_0 + \alpha\phi'_1 + O(\alpha^2),$$
$$\sigma' = \sigma'_0 + \alpha\sigma'_1 + O(\alpha^2). \tag{34}$$

Substituting this form of variables in Eqs. (24)–(26) and expressing the base-state conductivity given by Eq. (16) as $\overline{\sigma}(z) = 1 + \alpha\exp(-8z^2)$ yields the following leading order approximation of the governing equations:

$$\frac{\mathrm{Ra}_e}{\mathrm{Sc}}\frac{\partial}{\partial t}(\nabla^2\psi'_0) = \nabla^4\psi'_0 - \frac{\partial}{\partial z}\nabla^2\phi'_0, \tag{35}$$

$$\nabla^2\phi'_0 = \frac{\partial\sigma'_0}{\partial x}, \tag{36}$$

$$\frac{\partial\sigma'_0}{\partial t} - \frac{\partial\psi'_0}{\partial x}\frac{d\overline{\sigma}}{dz} = \frac{1}{\mathrm{Ra}_e}\nabla^2\sigma'_0. \tag{37}$$

Here we have retained $-(\partial\psi'_0/\partial x)d\overline{\sigma}/dz$ term, which is $O(\alpha)$, in the conductivity transport equation, Eq. (37), because $\mathrm{Ra}_e d\overline{\sigma}/dz$ is not small.

Next, we note that the leading order approximation of the perturbation free charge is given by $\rho'_{f0} = -\nabla^2\phi'_0$, from Gauss' law. Using this relation in Eq. (36) we can relate the free charge with the axial gradient of the conductivity as

$$\rho'_{f0} = -\frac{\partial\sigma'_0}{\partial x}. \tag{38}$$

Alternatively, the above relation can be obtained through leading order approximation of charge density given by Eq. (6). Also, the leading order term in the expansion of streamfunction, ψ'_0, is related to the vorticity ω'_0 as $\nabla^2\psi'_0 = -\omega'_0$. Here ω'_0 is the vorticity directed normal to the x-z plane and is positive for clockwise rotating flow. Therefore, the momentum equation, Eq. (35), can be written in terms of vorticity and free charge as

$$\frac{\mathrm{Ra}_e}{\mathrm{Sc}}\frac{\partial\omega'_0}{\partial t} = \nabla^2\omega'_0 - \frac{\partial\rho'_{f0}}{\partial z}. \tag{39}$$

Equation (38) suggests that the free charge builds up in the bulk solution primarily due to the axial conductivity gradients; there is no free charge in the base state. This free charge couples with the base-state electric field ($\hat{\mathbf{x}}$ in dimensionless form) to apply a torque $-\partial\rho'_{f0}/\partial z$ on the fluid, which generates a vorticity in the fluid, according to Eq. (39).

To test whether the approximate governing equations, Eqs. (37)–(39), correctly model the characteristics of EKI, we compare the eigenmodes and the critical Ra_e predicted using these equations with those presented in Fig. 3. Upon performing normal mode analysis of Eqs. (37)–(39) and noting that the critical state exhibits a stationary mode with $s = 0$, we obtain the following the following boundary value problem:

$$(D^2 - k^2)^2\hat{\psi}_0 = -D\hat{\rho}_{f0}, \tag{40}$$

$$\hat{\rho}_{f0} = -(D^2 - k^2)\hat{\phi}_0 = -ik\hat{\sigma}_0, \tag{41}$$

$$(D^2 - k^2)\hat{\sigma}_0 = -\mathrm{Ra}_e ik\hat{\psi}_0 D\overline{\sigma}, \tag{42}$$

with boundary conditions

$$\hat{\psi}_0 = D^2\hat{\psi}_0 = D\hat{\phi}_0 = \hat{\sigma}_0 = 0. \tag{43}$$

Here $\hat{\psi}_0(z)$, $\hat{\phi}_0(z)$, $\hat{\sigma}_0(z)$ are the eigenmodes corresponding to the eigenvalue Ra_e. Interestingly, this boundary value problem can also be expressed solely in terms of $\hat{\psi}_0$ as

$$(D^2 - k^2)^3\hat{\psi}_0 = \mathrm{Ra}_e k^2 D(D\overline{\sigma}\hat{\psi}_0), \tag{44}$$

with boundary conditions

$$\hat{\psi}_0 = D^2\hat{\psi}_0 = D(D^2 - k^2)^2\hat{\psi}_0 = 0. \tag{45}$$

We solved the eigenvalue problem described by Eqs. (40)–(42) with the boundary conditions (43) for $\gamma = 1.1$ and $\gamma = 1/1.1$. The wave numbers of the critical modes predicted using these equations and those using Eqs. (30)–(32) had a negligible difference of 0.01. Therefore, for comparison, we compare the eigenmodes of the exact and approximate linear models at critical k predicted by the exact model, Eqs. (30)–(32).

In Fig. 5 we present the critical eigenmodes predicted using the approximate model, Eqs. (40)–(42), for $\gamma = 1.1$, that is, when the center stream has higher conductivity than the sheath streams. The eigenmodes for conductivity and streamfunction shown in Fig. 5(a) are similar to those predicted using the actual linearized equations in Fig. 3(a). Moreover, the approximate model predicts $\mathrm{Ra}_e = 827.72$ at $k = 1.33$, comparable to the actual model's prediction of $\mathrm{Ra}_e = 863.27$. This suggests that the approximate model captures the essential physics of the instability.

Figure 5 also helps explain the destabilizing nature of the electric body force arising from the conductivity disturbance. The free charge density ρ'_{f0} plotted in Fig. 5(b) has similar sinuous structures as the eigenmode of conductivity σ'_0. However, ρ'_{f0} and σ'_0 have a phase difference along the x direction as $\rho'_{f0} = -\partial\sigma'_0/\partial x$ from Eq. (38). Alternatively, this can be deduced from Eq. (6), according to which the polarity of free charge is opposite to the directional derivative of σ along the electric field. Because the base-state electric field points along the axial direction, the free charge develops in the regions with axial conductivity gradients. The transverse gradients in the free charge result in a torque $-\partial\rho'_{f0}/\partial z$ on the fluid, shown in Fig. 5(c), which drives counter-rotating convection cells. As shown in Figs. 5(a) and 5(c), the directions of the torque and the rotation of the fluid are the same.

Similarly, in Fig. 6 we show the critical eigenmodes predicted using the simplified equations, Eqs. (40)–(42),

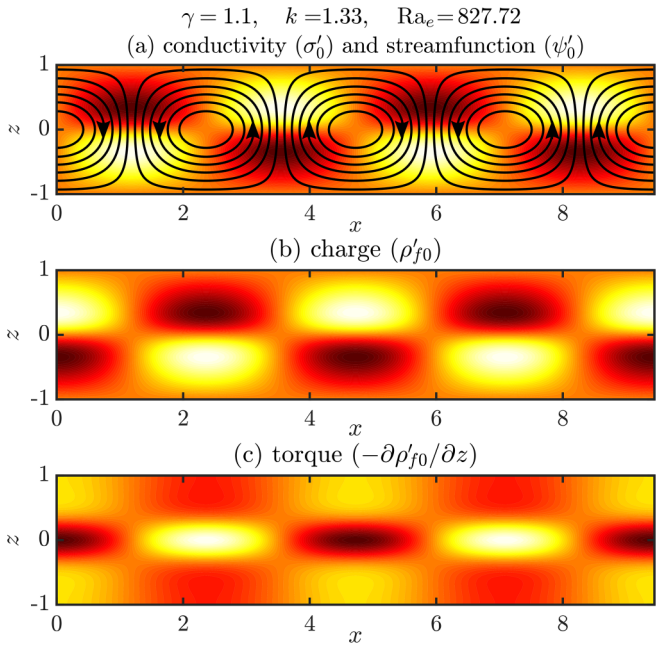

FIG. 5. The critical eigenmodes for $\gamma = 1.1$ predicted using the approximate equations for small conductivity difference between the center and sheath streams. Panel (a) shows the eigenmodes for conductivity σ_0' and the streamfunction ψ_0' (streamlines). Panels (b) and (c) show the corresponding free charge density ρ_{f0}' and torque $-\partial\rho_{f0}'/\partial z$, respectively. Yellow and red correspond to positive and negative perturbations, respectively. The torque's direction is consistent with fluid rotation within the convection cells.

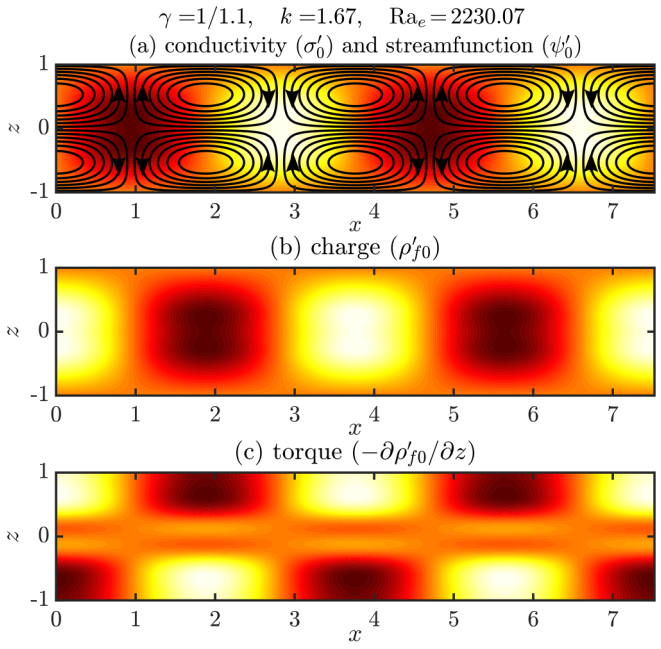

FIG. 6. Critical eigenmodes for $\gamma = 1/1.1$ predicted using the approximate equations based on small conductivity difference between the center and sheath streams. Panel (a) shows the eigenmodes for conductivity σ_0' and the streamfunction ψ_0' (streamlines). Panels (b) and (c) show the corresponding free charge density ρ_{f0}' and torque $-\partial\rho_{f0}'/\partial z$, respectively. Yellow and red correspond to positive and negative perturbations, respectively.

for $\gamma = 1/1.1$, that is, when the center stream has lower conductivity than the sheath streams. The eigenmodes for conductivity and streamfunction predicted using the approximate model, shown in Fig. 6(a), closely resemble those obtained using the actual model in Fig. 3(c). Also, the approximate model predicts $\mathrm{Ra}_e = 2230.07$ at $k = 1.67$, which is close to the actual value of $\mathrm{Ra}_e = 2011.99$. Because $\rho_{f0}' = -\partial\sigma_0'/\partial x$, the variation of free charge density ρ_{f0}' is similar to that of the conductivity disturbance, except for an axial phase difference. The torque associated with this charge density is shown in Fig. 5(c). In this case, the torque associated with the electric body force is antisymmetric about the center line $z = 0$. Therefore, it drives a pair of counter-rotating convection cells along the thickness of the fluid layer.

D. Physical mechanism

Having discussed the sinuous and varicose eigenmodes of EKI, we now summarize the physical mechanism underlying the selective appearance of these modes for different flow configurations. First, we consider the case with a high-conductivity center stream coflowing between two sheath streams ($\gamma > 1$). In Figs. 7(a) and 7(b),respectively, we illustrate the two possible conductivity disturbances for $\gamma > 1$: (i) sinuous disturbance, wherein the perturbations of the top and bottom conductivity interfaces are in-phase, and (ii) varicose disturbance, wherein the perturbations of the top and bottom interfaces are out of phase. The conductivity perturbations lead to gradients in the local electric field, which, in turn, due to Gauss' law, result in the accumulation of free charge in the bulk solution.

According to Eq. (38), the free charge is primarily governed by the axial conductivity gradients. The qualitative distribution of free charge corresponding to sinuous and varicose conductivity disturbances for $\gamma > 1$, based on Eq. (38), is illustrated in Figs. 7(a) and 7(b). The free charge associated with axial conductivity disturbances couples with the base-state electric field, applied along the x direction, to apply an electric body force on the fluid in the directions shown in Figs. 7(a) and 7(b). The variation of the electric body force along the transverse (z direction) results in a torque on the fluid that generates vorticity. The torque corresponding to the sinuous conductivity disturbance for $\gamma > 1$ drives vortices in a direction that further amplifies the conductivity perturbations, as shown in Fig. 7(a). This was also shown earlier in Fig. 5 using the approximate model derived in the limit of small conductivity difference between the flow streams. In contrast, a varicose conductivity disturbance for $\gamma > 1$ results in an electric body force, which is symmetric about the center line $z = 0$ and hence, the torque is antisymmetric about $z = 0$. Consequently, the torque drives a pair of counter-rotating vortices along the thickness of the fluid layer. These vortices diminish the amplitude of conductivity disturbances, as shown in Fig. 7(b). Therefore, EKI exhibits only the destabilizing sinuous mode when the center stream has higher conductivity than the sheath streams.

Next, in Figs. 7(c) and 7(d) we illustrate the physical mechanism of EKI in the configuration with the center stream having lower conductivity than the sheath streams ($\gamma < 1$). Because the free charge density is dictated by the axial conductivity gradients, the spatial distribution of charge due to

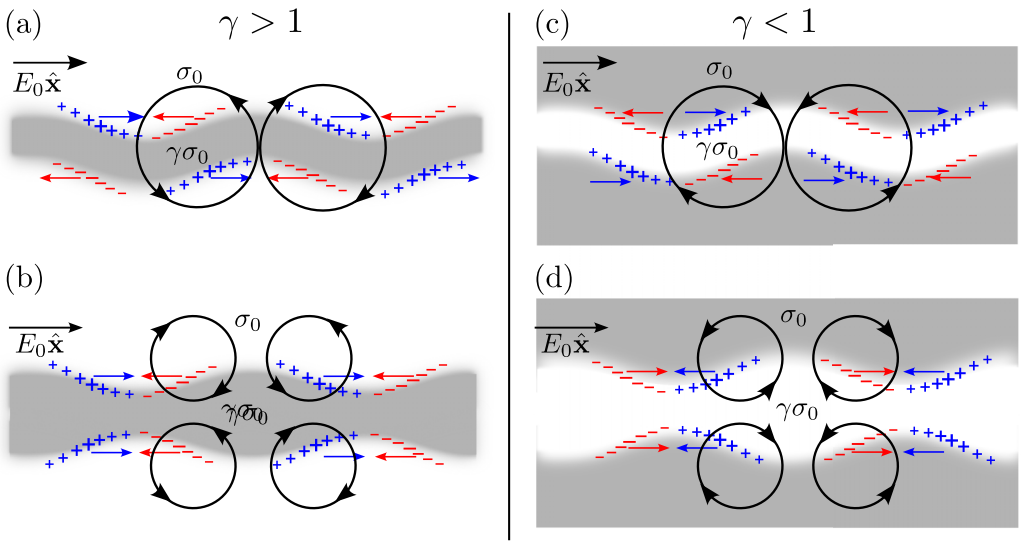

FIG. 7. Schematic illustrating the physical mechanism underlying selection of sinuous mode for higher conductivity and varicose mode for lower conductivity center streams. The flow is shown in the reference frame moving with uniform EOF. Negative charge accumulates in the region where the base-state electric field $E_0\hat{\mathbf{x}}$ crosses from a low- to high-conductivity region, whereas positive charge accumulates in the opposite case. The electric body force, due to the coupling of free charge and applied electric field, causes a torque that drives stationary convection cells. (a), (b) When the center has higher conductivity than the sheath streams ($\gamma > 1$), a sinuous conductivity disturbance leads to a destabilizing flow, as shown in (a), while a varicose disturbance induces a stabilizing flow, as shown in (b). (c), (d) When the center stream has lower conductivity than the sheath streams ($\gamma < 1$), the charge distribution and, hence, the EHD flow is opposite to that for $\gamma > 1$. Therefore, the sinuous disturbance, shown in (c), diminishes, and the varicose disturbance, shown in (d), amplifies.

conductivity disturbances for $\gamma < 1$ is opposite to that shown in Figs. 7(a) and 7(b) for $\gamma > 1$. Correspondingly, the torque resulting from coupling of the free charge and base-state electric field for $\gamma < 1$ is also opposite to that for $\gamma > 1$. Therefore, for $\gamma < 1$, the internal EHD flow generated due to a sinuous conductivity disturbance has a stabilizing effect, while the flow due to a varicose conductivity disturbance further amplifies the conductivity disturbance.

In summary, the crucial insight provided by Eq. (38), that the free charge in the bulk fluid develops primarily due to axial conductivity gradients, helps explain the destabilizing nature of sinuous and varicose conductivity disturbances for $\gamma > 1$ and $\gamma < 1$, respectively. Moreover, because a conductivity disturbance produces opposite charge distribution for base states with $\gamma > 1$ and $\gamma < 1$, the unstable and stable modes of one configuration are respectively stable and unstable for the other configuration. The physical mechanism of EKI described here explains why all experimental observations of EKI show only sinuous (varicose) mode when the center stream has higher (lower) conductivity than the sheath streams [14–16,19].

V. CONCLUDING REMARKS

We have performed a linear stability analysis of EKI in a system wherein EOF establishes a base-state flow with two sheath streams flowing in parallel with a center stream with mismatched electrical conductivity. In particular, we analyzed EKI for two distinct configurations where the center stream has higher or lower conductivity than the sheath streams. The stability analysis correctly explains the experimental observations of sinuous modes of EKI when the center stream has higher conductivity compared with the sheath streams and varicose modes for the opposite case. Moreover, the linear stability analysis predicts that the selection of unstable sinuous and varicose modes in the respective flow configurations is independent of the conductivity difference between the center and sheath streams.

We have also described the physical mechanism underlying the selection of sinuous and varicose modes of EKI in different flow configurations. The role of EOF in EKI is to establish the base state and convect the unstable modes. The instability occurs in form of stationary convection cells in the frame of reference moving with the EOF. The destabilizing flow is due to internal EHD motion driven by the coupling of the applied electric field with free charges associated with the conductivity gradients. Specifically, the spatial distribution of free charges is governed primarily by the axial conductivity gradients. Therefore, a conductivity disturbance over base states with center streams having higher and lower conductivity than the sheath streams produces opposite charge distribution in the regions with conductivity gradients. Consequently, the modes that are stable and unstable in the configuration with a higher conductivity stream in the center have an opposite effect in the configuration where the center stream has lower conductivity. Overall, the physical mechanism of EKI described here explains why all reported EKI experiments show either a sinuous or a varicose mode, depending upon the flow configuration.

ACKNOWLEDGMENTS

We acknowledge the financial support received from the Science and Engineering Research Board (SERB), Government of India, under the Mathematical Research Impact Centric Support (MATRICS) scheme (Grant No. MTR/2022/000080).

[1] P. Tabeling, *Introduction to Microfluidics* (Oxford University Press, New York, 2005).
[2] H. Masliyah and S. Bhattacharjee, *Electrokinetic and Colloid Transport Phenomena*, 3rd ed. (Wiley & Sons, New Jersey and Canada, 2006).
[3] C.-H. Chen and J. G. Santiago, A planar electroosmotic micropump, J. Microelectromech. Syst. **11**, 672 (2002).
[4] R. Bharadwaj and J. G. Santiago, Dynamics of field-amplified sample stacking, J. Fluid Mech. **543**, 57 (2005).
[5] S. S. Bahga and J. G. Santiago, Coupling isotachophoresis and capillary electrophoresis: A review and comparison of methods, Analyst **138**, 735 (2013).
[6] M. H. Oddy, J. G. Santiago, and J. C. Mikkelsen, Electrokinetic instability micromixing, Anal. Chem. **73**, 5822 (2001).
[7] K. Dubey, S. Sanghi, A. Gupta, and S. S. Bahga, Electrokinetic instability due to streamwise conductivity gradients in microchip electrophoresis, J. Fluid Mech. **925**, A14 (2021).
[8] R. Gaur and S. S. Bahga, Electrohydrodynamic instability of ion-concentration shock wave in electrophoresis, Phys. Rev. E **95**, 063109 (2017).
[9] J. F. Hoburg and J. R. Melcher, Internal electrohydrodynamic instability and mixing of fluids with orthogonal field and conductivity gradients, J. Fluid Mech. **73**, 333 (1976).
[10] C.-H. Chen, H. Lin, S. K. Lele, and J. G. Santiago, Convective and absolute electrokinetic instability with conductivity gradients, J. Fluid Mech. **524**, 263 (2005).
[11] S. Sharan, P. Gupta, and S. S. Bahga, Mechanism of electrohydrodynamic instability with collinear conductivity gradient and electric field, Phys. Rev. E **95**, 023103 (2017).
[12] J. R. Melcher and W. J. Schwarz, Jr., Interfacial relaxation overstability in a tangential electric field, Phys. Fluids **11**, 2604 (1968).
[13] J. D. Zahn and V. Reddy, Two phase micromixing and analysis using electrohydrodynamic instabilities, Microfluid. Nanofluid. **2**, 399 (2006).
[14] J. D. Posner, C. L. Pérez, and J. G. Santiago, Electric fields yield chaos in microflows, Proc. Natl. Acad. Sci. USA **109**, 14353 (2012).
[15] S. Shin, I. Kang, and Y.-K. Cho, Mixing enhancement by using electrokinetic instability under time-periodic electric field, J. Micromech. Microeng. **15**, 455 (2005).
[16] J. D. Posner and J. G. Santiago, Convective instability of electrokinetic flows in a cross-shaped microchannel, J. Fluid Mech. **555**, 1 (2006).
[17] N. A. Patankar, Electrokinetic instability: The sharp interface limit, Phys. Fluids **23**, 014101 (2011).
[18] H. Lin, Electrokinetic instability in microchannel flows: A review, Mech. Res. Commun. **36**, 33 (2009).
[19] K. Dubey, A. Gupta, and S. S. Bahga, Coherent structures in electrokinetic instability with orthogonal conductivity gradient and electric field, Phys. Fluids **29**, 092007 (2017).
[20] H. Bruus, *Theoretical Microfluidics* (Oxford University Press, Oxford, 2008).
[21] M. Babar, K. Dubey, and S. S. Bahga, Effect of surface conduction–induced electromigration on current monitoring method for electroosmotic flow measurement, Electrophoresis **41**, 570 (2020).
[22] H. Lin, B. D. Storey, M. H. Oddy, C.-H. Chen, and J. G. Santiago, Instability of electrokinetic microchannel flows with conductivity gradients, Phys. Fluids **16**, 1922 (2004).
[23] K. Swinney and D. J. Bornhop, Quantification and evaluation of Joule heating in on-chip capillary electrophoresis, Electrophoresis **23**, 613 (2002).
[24] A. Persat and J. G. Santiago, An Ohmic model for electrokinetic flows of binary asymmetric electrolytes, Curr. Opin. Colloid Interface Sci. **24**, 52 (2016).
[25] S. Chandrasekhar, *Hydrodynamic and Hydromagnetic Stability* (Dover Publications, New York, 1981).
[26] J. P. Boyd, *Chebyshev and Fourier Spectral Methods* (Courier Corporation, 2001).
[27] M. H. Chang, A. C. Ruo, and F. Chen, Electrohydrodynamic instability in a horizontal fluid layer with electrical conductivity gradient subject to a weak shear flow, J. Fluid Mech. **634**, 191 (2009).